

Geospatial Mapping of Short-Term Particulate Matter Measurements using Small Unmanned Aircraft Systems (sUAS).

Daniel K. Boey^{1,2}, David W. Johnston²

¹Division of Marine Science and Conservation, Nicholas School of the Environment, Duke University, Beaufort, USA.

²Pratt School of Engineering, Duke University, Durham, USA.

Submitted as part of requirements for Research Independent Study.

ABSTRACT

Particulate matter (PM) is often used as a key indicator of the air pollution due to its adverse impact on human health. Small unmanned aircraft systems (sUAS) allow PM to be monitored rapidly and with ease in a variety of situations previously inaccessible to manned systems. The advent of lightweight, low-cost PM sensors also allows for drone-mounted air quality sensors. A PM_{2.5} sensor was mounted on a sUAS and programmed to fly along programmed waypoints. Initial flights confirmed by wind testing detected directional biases associated with the sensor, likely due to prevalent winds in flight. Biases were overcome by programming the drone to circle on the spot at each waypoint, thereby compensating for any detection bias. This study proves the feasibility and effectiveness of using sUAS to geospatially map short-term PM measurements.

I. INTRODUCTION

Air pollution has been consistently associated with many acute and chronic health problems which largely depends on the type and extent of pollutant exposure (Brook et al., 2004; Cohen et al., 2005). A comparison of the risks and disability-adjusted life-years (DALYs) reviewed that household air pollution and ambient PM contributed to an estimate of over 5.5 million premature deaths in 2013 and 141.5 million DALYs (Forouzanfar et al., 2015). Other than gaseous particles, PM remains one of the most important aerosol particles emitted by human activities and inhaled by humans (Amaral, de Carvalho, Costa, & Pinheiro, 2015). Studies have shown that exposure to PM_{2.5} levels from over a few hours to a few years can dramatically increase individuals' risk for a series of cardiovascular diseases, mortality and other related nonfatal events (Brook et al., 2010; Du, Xu, Chu, Guo, & Wang, 2016). This is especially prevalent when analyzing PM related health risks across a population (Martinelli, Olivieri, & Girelli, 2013). As such, PM is often used as a standard indicator of air pollution. The European Union, United States' Environmental Protection Agency, and the World Health Organization have set PM standards in recognition of its impact on human health (Environment Directorate General of the European Commission, 2017; United States Environmental Protection Agency, 2016; World Health Organization, 2006).

Spatial mapping has the potential to increase public awareness of daily pollutant exposure. Residents are not always aware of the potentially hazardous air quality levels or the major pollutant sources present in their area (Brody, Peck, & Highfield, 2004). Public risk perception is critical in galvanizing support for effective environmental policies that the government can undertake. Being aware of citywide air quality data would help local governments target pollutant sources to mitigate air pollution and protect human health. Furthermore, spatial reasoning remains critical in easing the decision-making process when different types of data can be displayed simultaneously. One example is to present the background and processes of scientific information at a single glance (An et al., 2014). Data visualization achieves this by facilitating the integration of multiple geographical, air quality, and socio-economic databases onto a single user interface.

However, PM levels is heavily subject to the dynamic processes in the atmosphere from the local level to the global level and the interactions that occur between them (Monks et al., 2009). To better understand human exposure to harmful gaseous pollutants and climate aerosols, accurate and relevant measurements are required (Villa, Gonzalez, Miljevic, Ristovski, & Morawska, 2016). Current methods of ground, manned aircraft as well as via satellite imagery still prove insufficient to obtain data of spatial and temporal resolutions sufficient to understand human exposure and take effective action (Miller et al., 2011).

Fortunately, unmanned Aerial Systems (UAS) provide a new frontier in assessing and visualizing local air quality data. UAS bring the capability to provide measurements at high spatiotemporal resolutions with relatively low-costs (Messinger & Silman, 2016). Its versatility is rooted in its applicability to a host of contexts, especially into hazardous conditions that rule out ground or manned vehicular methods. This includes detecting gas or chemical emissions and forests fires (Amaral et al., 2015; Neumann, Hernandez Bennetts, Lilienthal, Bartholmai, & Schiller, 2013; Zhou, Aurell, Mitchell, Tabor, & Gullett, 2017).

This study provides a framework for the usage of sUAS (small UAS), specifically quadcopters, to reliably measure the amount of PM in the air. By integrating PM measurements and Geographical Positioning System (GPS) data, a geospatial map of the air quality across a defined area can be rapidly obtained, thereby proving the feasibility of using sUAS to geospatially map air quality indicators across the area of interest.

II. METHODOLOGY

The drone employed for the purposes of the study will be the 3DR IRIS+ Quadcopter (3DR) henceforth referred to the drone for brevity (Figure 1). It has a flight time of between 15-20 minutes and can be easily programmable using opensource software such as Mission Control (UgCS). This allows autonomous flight planning and precision flying, both of which are integral for mapping work.


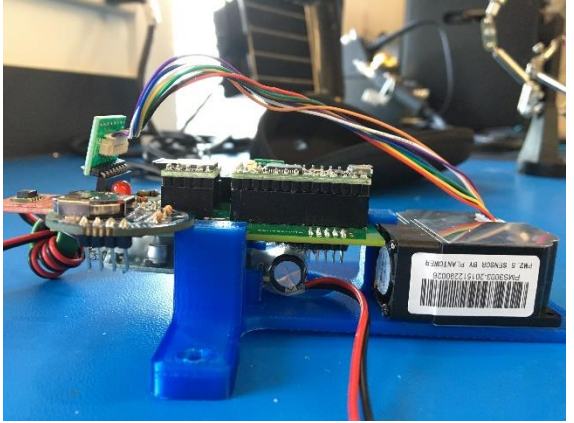
3DR IRIS+ Quadcopter	Plantower 3003 PM _{2.5} sensor with 3.2 Teensy Microcontroller
	
Pixhawk-based Quadcopter 3-cell 11.1 3.5Ah LiPo Battery Radio range: 1km Max. Flight Time: 10-13 minutes Payload: 425g Estimated cost: US\$550	Arduino-based PM Sensor 5V DC Supply Voltage (drawn from drone) Parameters: Index/unit ($\mu\text{g}/\text{m}^3$) Estimated cost: US\$50

Figure 1: Specifications of 3DR IRIS+ Quadcopter and Plantower 3003 PM_{2.5} sensor with 3.2 Teensy Microcontroller

The PM sensor is a Plantower 3003 PM_{2.5} sensor (Plantower). PM_{2.5} concentration levels are measurements of all solid and liquid particles that are suspended in the air with a diameter of less than 2.5 microns. The sensor is a laser-scattering device that is connected to a 3.2 Teensy USB-based microcontroller development board. The sensor logs PM_{2.5}, temperature and relative humidity, amongst other measurements onto a microSD card mounted onto the sensor. Due to the delays involved in recording data, the highest frequency of PM_{2.5} data that can be obtained is 0.5-1 Hz. Data is then downloaded from the microSD card for analysis.

A. SENSOR MOUNTING & INTEGRATION

A 3D-printed sensor mount was designed and created to fit the 3.2 Teensy USB microcontroller board and Plantower sensor. This enables the components of the system to be securely held together as one unit. Using screws available on the underbelly of the drone, the sensor mount was secured. The 5V power required for the sensor will come from the drone's power source via servo leads. It is noteworthy that the system did not draw much power and had little effect on the maximum flight time of the drone.



Figure 2: IRIS+ Quadcopter with Plantower PM_{2.5} sensor mounted.

B. PROGRAMMING

Both the drone and PM sensor had to be programmed for the purposes of air quality measurement flights.

To enable autonomous flying, the drone was programmed using an open source software called Mission Planner. This includes creating GPS way points, using pre-set drone behaviors (continuous flying, loitering, circling, etc.) and establishing parameters the drone abides by (speed, altitude, rate of climb, rate of rotation, etc.). These data can be uploaded into the drone and continually tracked using the Mission Planner application on a computer or a tablet via datalinks.

The Arduino-based Teensy microcontroller receives data from the PM sensor and writes [it](#) onto a MicroSD card. For the purposes of this experiment, the sensor was programmed to write data every 1-2 seconds which provides a finer temporal scale of the PM. Data collection is limited by the maximum flight time of the drone and therefore measurements were taken continuously to maximize data obtained.

C. UAS FLIGHTS

Once datalink and GPS lock are established, the drone flies according to the pre-set waypoints and parameters. A return-to-home command can also be set, allowing the drone to autonomously fly from start to end. During the whole flights, the pilot-in-command of the drone is always alert for any aerial interferences or unplanned deviances and can switch to manual control of the drone through the remote controller.

Initial flights were planned to use a surveying grid within Mission Planner. The area to be surveyed was gridded up and the desired altitude, speed and surveying overlap were defined. the software automatically plans the way points and path taken by the drone.

D. DATA PROCESSING & MANIPULATION

Data will be obtained from two sources: drone flight logs and data recorded from the sensor. The sensor records PM_{2.5} concentration level data in a comma delimited format and can be easily manipulated using MATLAB. Data from the drone arrives in *.kmz*, *.gpx* and *.log* files which require further processing to be manipulatable. Within the sensor data, the random time lags due to the printing of data onto the microSD card in a *.txt* file causes the data obtained to be irregular (~0.5-1 Hz).

Also, with the irregular gaps in the high frequency of GPS data (~10Hz) and relatively low frequency of PM data (~0.5-1 Hz), methods must be employed to obtain a valid and reliable sync between the two types of data. Additionally, the manual connection required to switch on and off the PM sensor made it possible to start and end data collection only when the UAS was on the ground. It is noteworthy that the first ~20s of data was disregarded as the drone often took time to move to its starting point and return to land. This can be easily eliminated using elevation data from the drone.

In MATLAB, a regular time series of 1 Hz was created from the start and end timing. Data was then drawn from GPS and PM data. Due to the fine spatiotemporal resolution of GPS data, only the first point within every second was used to represent the GPS position of the UAS aircraft. For gaps within the air quality data or when the difference between two subsequent data points was 2s, linear interpolation was employed to fill the gaps. This enabled a synced spatiotemporal data series to be obtained.

E. GEOSPATIAL MAPPING

The synced spatiotemporal data was then uploaded into ArcGIS to create a 2D plot of the air quality. The WGS1984 Geographic Projection System and a satellite-based base map was used.

F. WIND TESTING

Initial flights showed that the sensor was likely to have directional biases. This can be deduced from the visual geospatial map from initial flights (Figure 2). With a dominant North-Easterly wind during that day of flight, air quality was significantly better when the drone and sensor were moving

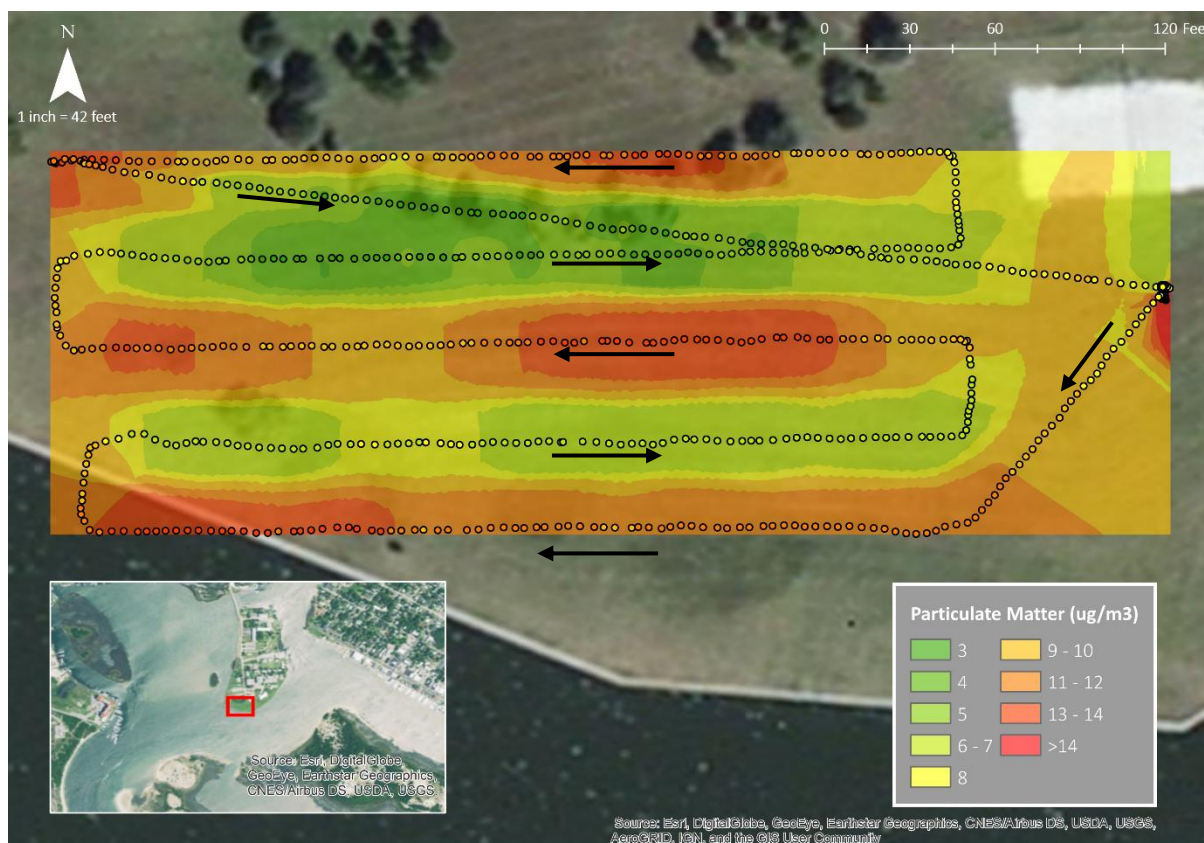


Figure 3: Geospatial map of an initial flight showing direction biases at Pivers Island. Each dot represents one data point including PM, latitude, and longitude data. Shading and data point marker colors are identical, as shown in the legend. Arrows represent the direction of the movement of drone. Higher levels of PM were obtained when the drone was moving towards the West. Note that the inlet of the sensor was facing towards the aft of the UAS (i.e. facing in the opposite direction of the drone).

westwards than when they were moving eastwards. As a result, further analysis was required to confirm the hypothesis that the sensor recorded higher PM levels when wind was blowing against the sensor's rear (towards the fan of the sensor).

III. RESULTS AND DISCUSSION

A. DIRECTIONAL BIASES

Initial flights and tests showed that the sensor possessed directional biases. The geospatial map obtained from a continuous flight showed that the sensor recorded higher levels of PM when the drone was moving towards the west (Figure 3). The easterly wind recorded on the day at about 9 mph was sufficient to cause directional biases to arise. In other words, the sensor recorded higher PM levels when the wind was blowing against the rear of the sensor (where the fan was located). To confirm this observation, a stationary test involving the sensor, simulated wind and simulated PM was conducted.

In this experiment, the sensor was placed on a compass that allowed us to vary the angle of wind blowing against the sensor. A large fan of was employed to simulate wind. Four incense sticks of height xx mm within a bucket were burnt to simulate PM. The bucket was used to channel the PM into the channel of wind created by the fan. Incense was placed in between the bucket and the fan, causing the fan to push PM towards the sensor. The zero degrees position represented that the sensor's inlet was facing the wind and the incense whilst 180 degrees position represented that the sensor's rear was facing the wind and the incense.

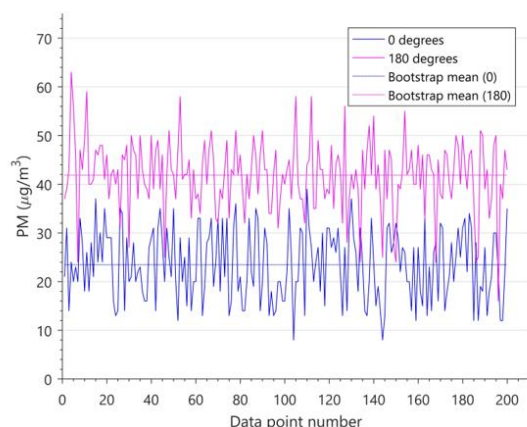


Figure 4 (L): Graph comparing $PM_{2.5}$ levels between 0 and 180 degrees position with bootstrap mean of the respective positions.

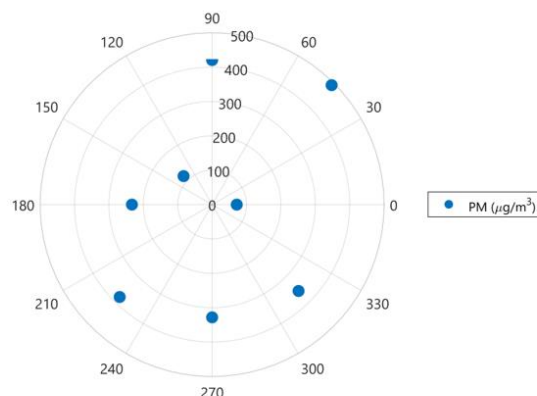


Figure 5 (R): Polar scatter plot showing $PM_{2.5}$ mean at 45-degree interval positions.

To confirm bidirectional biases, the sensor recorded six minutes of data each (~200 samples) in the 0 and 180 degrees positions. Bootstrapping of ten thousand iterations was employed to obtain a bootstrap mean as well as the 95 percent and 5 percent confidence intervals. It was found that the mean $PM_{2.5}$ level was almost two times higher at the 180 degrees position as compared to the 0 degrees position (Table 6, Figure 4). A standard t-test was employed and found a statistical difference between the two positions.

	Simple mean	Standard deviation	Bootstrap mean	5% confidence interval	95% confidence interval
0 degrees	23.5	7.24	23.5	22.6	24.3
180 degrees	41.9	7.23	41.9	41.0	42.7

Table 6: Statistical information of 0 and 180 degrees position ($\mu g/m^3$)

We hypothesize that the difference in levels recorded between the two positions is due to changes in flow rate within the sensor. Due to restrictions on proprietary information, the manufacturer of the Plantower sensor did not release information on the mechanisms of the sensor. The fan is likely to maintain a predetermined flow rate of air flowing through the sensor, allowing the laser to record the number of PM that scatter light. The central processing unit of the sensor can then calculate the $PM_{2.5}$ levels by the following equation.

$$C = \frac{N}{Q} \quad (1)$$

where C is the calculated $PM_{2.5}$ concentration level, N is the number of particles present in a fixed volume per unit time and Q is the pre-determined volumetric flow rate.

Resultantly, as wind blows against the fan at the rear of the sensor, the ability of the fan to maintain the flow rate is impeded. Thus, the flow rate of the actual air flowing through the sensor will be less than the fixed Q the sensor assumes (Equation 1). Therefore, $PM_{2.5}$ levels are artificially inflated.

Furthermore, PM data of one-minute intervals was taken for positions at 45-degree intervals (Figure 5). An omnibus circular statistic test was employed ($p\text{-val} < 1e-10$), suggesting that the data is not uniform across the circle. However, due to the lack of uniformity of PM experienced by the sensor at one given point of time, this could be attributed to a lack of uniform experimental conditions than actual sensor biasness.

B. GEOSPATIAL MAPPING

To overcome the directional biases, waypoint flying was employed. The drone will be programmed to move sequentially to predetermined GPS waypoints, taking advantage of its capability as a rotary wing UAS to hover. At these waypoints, the drone was programmed to rotate 360 degrees on the spot at a rate of 18 degrees per second for a total of 20 seconds. A hovering flight of 8 minutes was conducted. From the data, auto-correlation coefficients for each lag value were calculated using the following equation:

$$r_k = \frac{\sum_{t=k+1}^N (r_t - \bar{r})(r_{t-k} - \bar{r})}{\sum_{t=1}^N (r_t - \bar{r})^2} \quad (2)$$

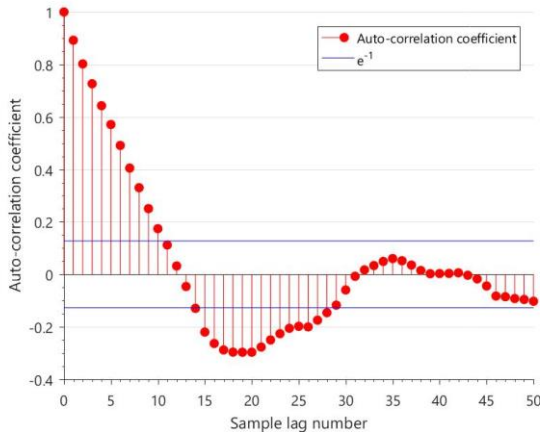


Figure 7: Graph of auto-correlation coefficients against lag numbers.

where N is the total number of samples, r is the data set elements, k is the lag number and \bar{r} is the mean value of the data set.

It was found that auto-correlation coefficients decayed below e^{-1} after 12 samples (Figure 7). Since the sampling rate is ~ 0.60 Hz, the coefficients took roughly 20s before decaying below e^{-1} . 20s. In other words, the data was no longer correlated with itself after 20s, which gives us the optimal time to record data at a singular point. After which, all variation in mean may be attributed to random elements rather than giving us a better representation of $PM_{2.5}$ concentration levels.

30 waypoints were set above Pivers Island in a 5×6 grid with a difference of 0.0004 degrees in latitude and 0.0005 degrees in longitude between each waypoint. The drone completed data collection over two flights of ~ 8 minutes flight time each to obtain the geospatial map (Figure 8). Whilst 30 points may be insufficient to give an accurate or useful interpolation within the grid space, it is possible to use various spatial analyst tools available in ArcGIS to show PM trends across the experimental area.



Figure 8: Geospatial map of 20s mean $PM_{2.5}$ concentration levels at 30 distinct points over Pivers Island, NC. There was slightly higher $PM_{2.5}$ levels over the main buildings over the island.

IV. CONCLUSION

This study proves the feasibility and effectiveness of using sUAS to geospatially map short-term PM concentration levels. The current findings suggest that the current low-cost sensors are still inadequate in their ability to account for directional biases which has a significant effect on the measurements and results of the study. Hence, further sensor design and research are required to create a system that could increase the efficiency and effectiveness of using sUAS for air quality mapping work. Once we can eliminate such biases, the drone could record and transmit air quality data continuously back to the user, allowing real time information to be recorded and sent. Given technological advancements in drone programming and aerodynamics, the range and flight accuracy of sUAS will undoubtedly increase. Resultantly, this unlocks possibilities of air quality mapping across densely populated cities, industrial regions and more.

REFERENCES

- Amaral, S. S., de Carvalho, A. J., Costa, A. M., & Pinheiro, C. (2015). An Overview of Particulate Matter Measurement Instruments. *Atmosphere*, 6(9). doi:10.3390/atmos6091327
- An, S. M., Lee, H.-Y., Kim, B., Yi, C.-Y., Eum, J.-H., & Woo, J.-H. (2014). Geospatial spreadsheets with microscale air quality visualization and synchronization for supporting multiple-scenario visual collaboration. *International Journal of Geographical Information Science*, 28(12), 2511-2532. doi:10.1080/13658816.2014.938077
- Brody, S. D., Peck, B. M., & Highfield, W. E. (2004). Examining Localized Patterns of Air Quality Perception in Texas: A Spatial and Statistical Analysis. *Risk Analysis*, 24(6), 1561-1574. doi:10.1111/j.0272-4332.2004.00550.x
- Brook, R. D., Franklin, B., Cascio, W., Hong, Y. L., Howard, G., Lipsett, M., . . . Tager, I. (2004). Air pollution and cardiovascular disease - A statement for healthcare professionals from the expert panel on population and prevention science of the American Heart Association. *Circulation*, 109(21), 2655-2671. doi:10.1161/01.Cir.0000128587.30041.C8
- Brook, R. D., Rajagopalan, S., Pope, C. A., Brook, J. R., Bhatnagar, A., Diez-Roux, A. V., . . . Metab, C. N. P. A. (2010). Particulate Matter Air Pollution and Cardiovascular Disease An Update to the Scientific Statement From the American Heart Association. *Circulation*, 121(21), 2331-2378. doi:10.1161/CIR.0b013e3181d8e1
- Cohen, A. J., Ross Anderson, H., Ostro, B., Pandey, K. D., Krzyzanowski, M., Künzli, N., . . . Smith, K. (2005). The Global Burden of Disease Due to Outdoor Air Pollution. *Journal of Toxicology and Environmental Health, Part A*, 68(13-14), 1301-1307. doi:10.1080/15287390590936166
- Du, Y., Xu, X., Chu, M., Guo, Y., & Wang, J. (2016). Air particulate matter and cardiovascular disease: the epidemiological, biomedical and clinical evidence. *Journal of Thoracic Disease*, 8(1), E8-E19. doi:10.3978/j.issn.2072-1439.2015.11.37
- Environment Directorate General of the European Commission. (2017). Air Quality Standards. Retrieved from <http://ec.europa.eu/environment/air/quality/standards.htm>
- Forouzanfar, M. H., Alexander, L., Anderson, H. R., Bachman, V. F., Biryukov, S., Brauer, M., . . . Murray, C. J. (2015). Global, regional, and national comparative risk assessment of 79 behavioural, environmental and occupational, and metabolic risks or clusters of risks in 188 countries, 1990-2013: a systematic analysis for the Global Burden of Disease Study 2013. *Lancet*, 386(10010), 2287-2323. doi:10.1016/s0140-6736(15)00128-2
- Martinelli, N., Olivieri, O., & Girelli, D. (2013). Air particulate matter and cardiovascular disease: A narrative review. *European Journal of Internal Medicine*, 24(4), 295-302. doi:<https://doi.org/10.1016/j.ejim.2013.04.001>
- Messinger, M., & Silman, M. (2016). Unmanned aerial vehicles for the assessment and monitoring of environmental contamination: An example from coal ash spills. *ENVIRONMENTAL POLLUTION*, 218, 889-894. doi:10.1016/j.envpol.2016.08.019
- Miller, D. J., Sun, K., Zondlo, M. A., Kanter, D., Dubovik, O., Welton, E. J., . . . Ginoux, P. (2011). Assessing boreal forest fire smoke aerosol impacts on U.S. air quality: A case study using multiple data sets. *Journal of Geophysical Research: Atmospheres*, 116(D22), D22209. doi:10.1029/2011JD016170
- Monks, P. S., Granier, C., Fuzzi, S., Stohl, A., Williams, M. L., Akimoto, H., . . . von Glasow, R. (2009). Atmospheric composition change – global and regional air quality. *ATMOSPHERIC ENVIRONMENT*, 43(33), 5268-5350. doi:<https://doi.org/10.1016/j.atmosenv.2009.08.021>
- Neumann, P. P., Hernandez Bennetts, V., Lilienthal, A. J., Bartholmai, M., & Schiller, J. H. (2013). Gas source localization with a micro-drone using bio-inspired and particle filter-based algorithms. *Advanced Robotics*, 27(9), 725-738. doi:10.1080/01691864.2013.779052
- United States Environmental Protection Agency. (2016). NAAQS Table. Retrieved from <https://www.epa.gov/criteria-air-pollutants/naaqs-table>
- Villa, T. F., Gonzalez, F., Miljevic, B., Ristovski, Z. D., & Morawska, L. (2016). An Overview of Small Unmanned Aerial Vehicles for Air Quality Measurements: Present Applications and Future Prospectives. *Sensors*, 16(7), 1072-1072. doi:10.3390/s16071072
- World Health Organization. (2006). *WHO Air quality guidelines for particulate matter, ozone, nitrogen dioxide and sulfur dioxide*. Retrieved from http://apps.who.int/iris/bitstream/10665/69477/1/WHO_SDE_PHE_OEH_06.02_eng.pdf
- Zhou, X. C., Aurell, J., Mitchell, W., Tabor, D., & Gullett, B. (2017). A small, lightweight multipollutant sensor system for ground-mobile and aerial emission sampling from open area sources. *ATMOSPHERIC ENVIRONMENT*, 154, 31-41. doi:10.1016/j.atmosenv.2017.01.029